Electronic Supplementary Information (ESI)

High stretchable, bionic self-healing waterborne polyurethane elastic film enabled by multiple hydrogen bonding for flexible strain sensors

Ending Zhang [a, b], Xiaohong Liu [a, b], Yingchun Liu [a, b], Jun Shi [a, b, f, *], Xiaobin Li [a, b], Xiaoyan Xiong [a, b], Changan Xu [a, b, c], Kun Wu [a, b, e], Mangeng Lu [a, b, d]

[a] *Guangzhou Institute of Chemistry, Chinese Academy of Sciences, Guangzhou 510650, People's Republic of China.*

[b] *University of Chinese Academy of Sciences, Beijing 10049, People's Republic of China.*

[c] *CAS Engineering laboratory for Special Fine Chemicals, Guangzhou 510650, People's Republic of China.*

[d] *Guangdong Provincial Key Laboratory of Organic Polymer Materials for Electronics, Guangzhou 510650, People's Republic of China.*

[e] *CASH GCC Shaoguan Research Institute of Advanced Materials.*

[f] *New Materials Research Institute of CASCHEM (Chongqing) Co., Ltd, Chongqing, 400714, People's Republic of China.*

*Corresponding author, E-mail address: junshi@gic.ac.cn (Jun Shi).

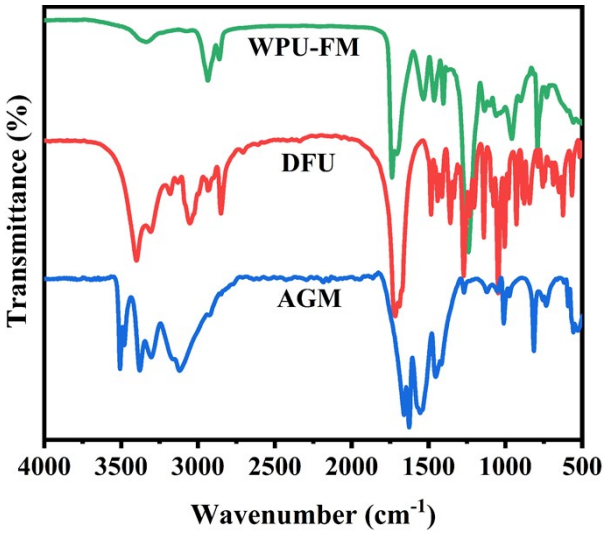

Figure S1. FTIR spectra of WPU-FM, DFU and AGM.

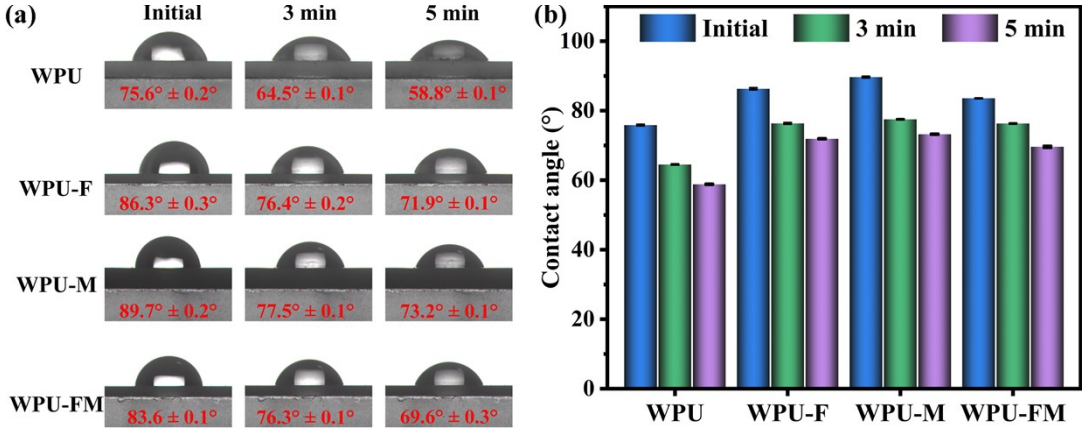

Figure S2. Images (a) and data bar charts (b) of contact angle of WPU, WPU-F, WPU-M, WPU-FM films in different periods.

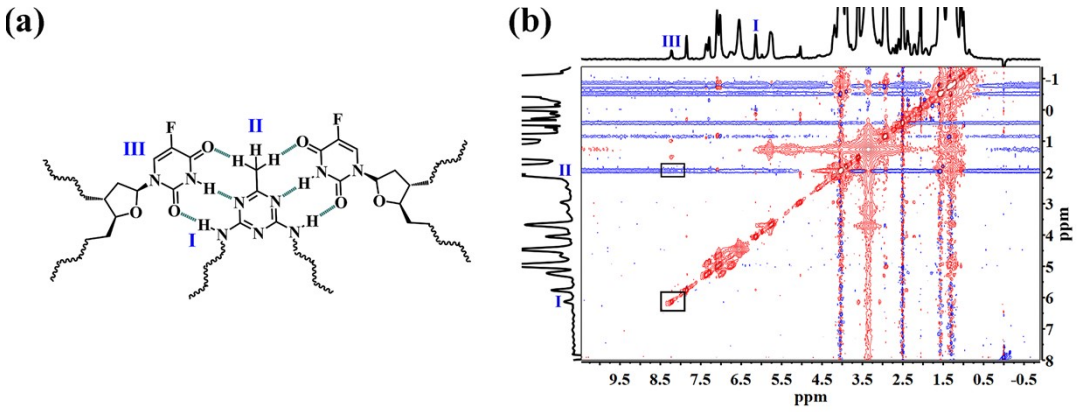

Figure S3. Theoretical structure model of six-fold hydrogen bonds (a), NOESY NMR spectrum of WPU-FM sample (b).

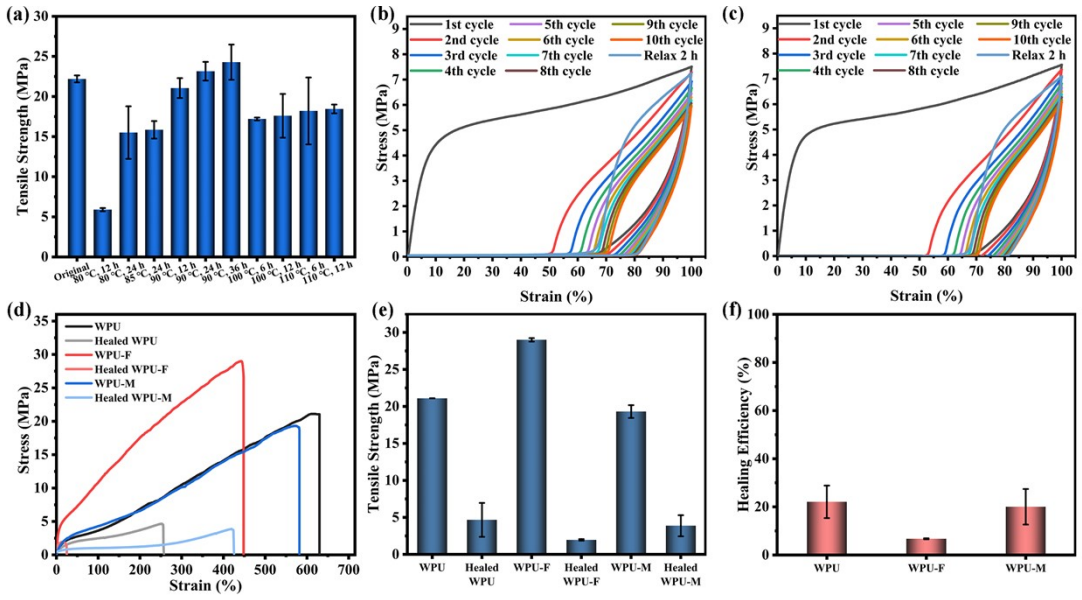

Figure S4. Tensible strength of WPU-FM sample healed under various conditions (a). The cyclic tensile curves of WPU-FM film healed at 90 °C for 12 h (b), and of the original sample (c), when the strain was 100%. The mechanical properties (d-e) and healing efficiency (f) of WPU, WPU-F and WPU-M film healed at 90 °C for 12 h.

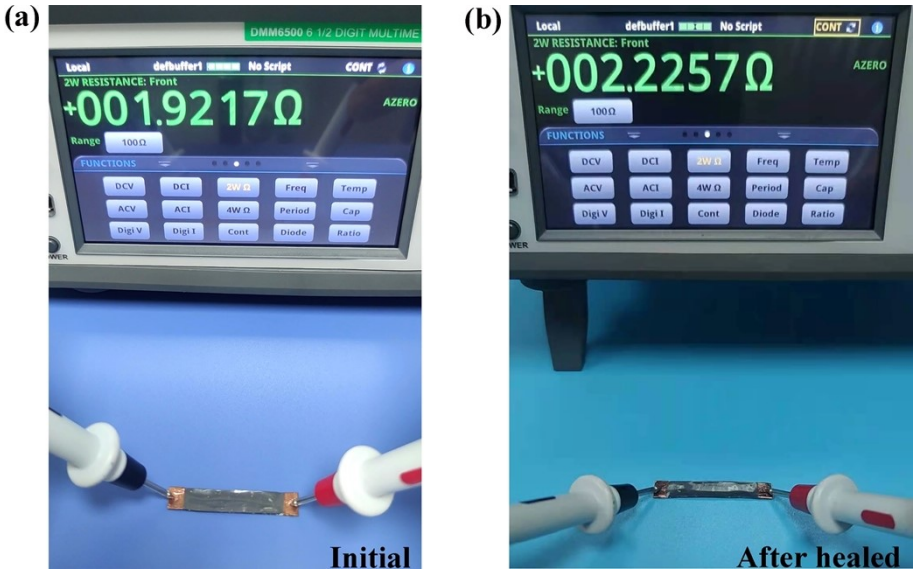

Figure S5. The resistance value (R) of the initial WPU-FM/LM (a) and the healed WPU-FM/LM (b).

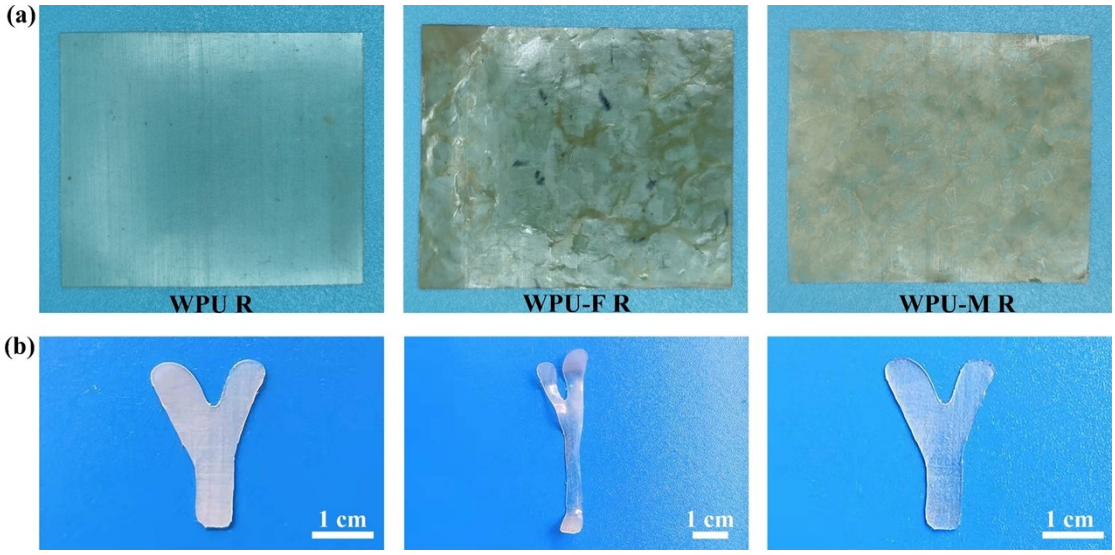

Figure S6. Photographs of WPU R, WPU-F R and WPU-M R film after secondary processing (a). Demonstration of shape memory performance of "Y" shape WPU-FM film (b).

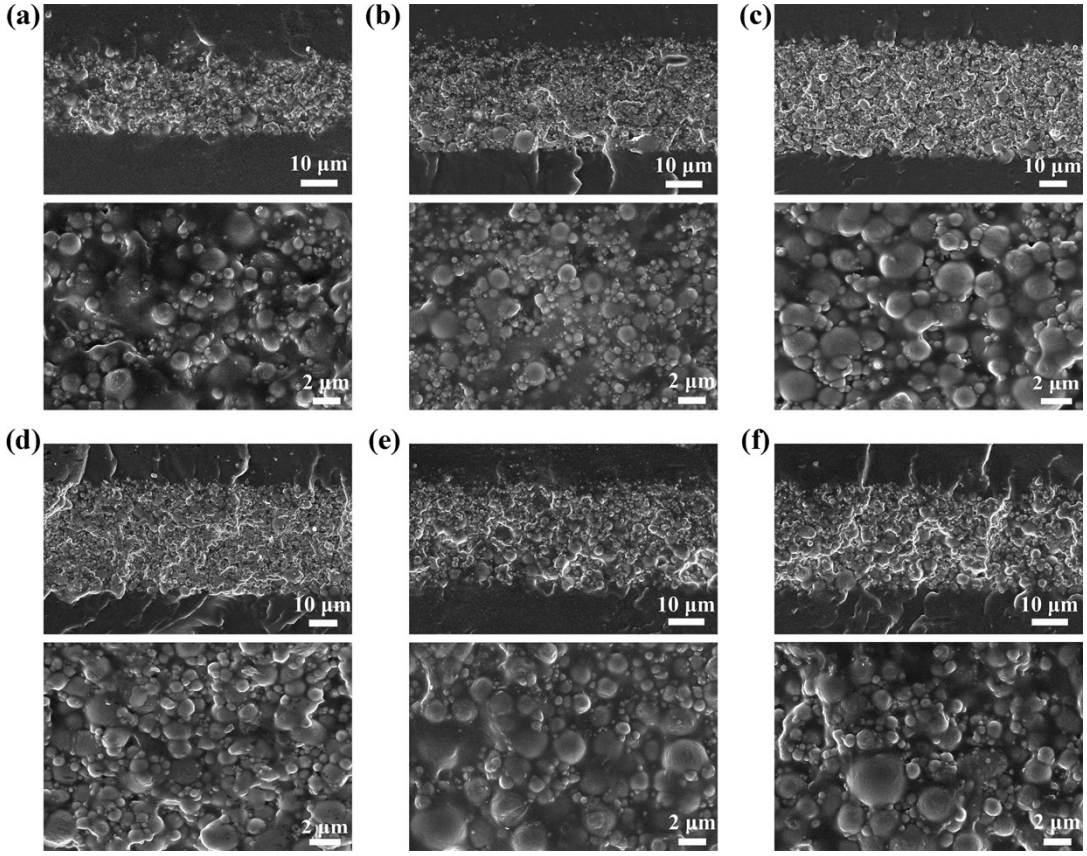

Figure S7. SEM images of the cross-sectional morphology of WPU-FM/LM composite films (LM: 25 wt.% (a), 30 wt.% (b), 35 wt.% (c), 40 wt.% (d), 45 wt.% (e) and 50 wt.% (f).).

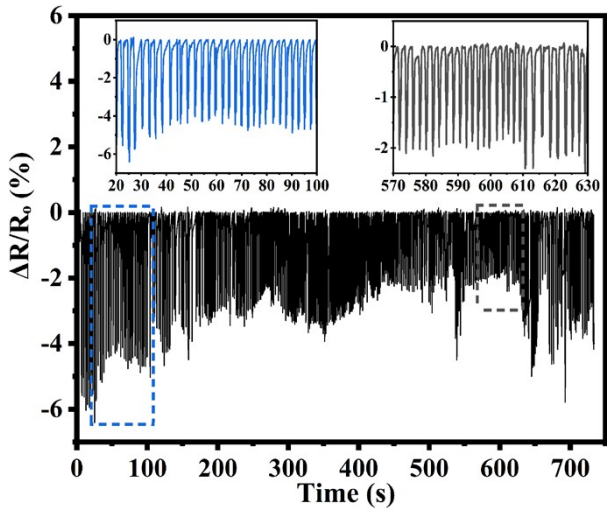

Figure S8. $\Delta R/R_0$ vs time of right index finger bend 365 times.

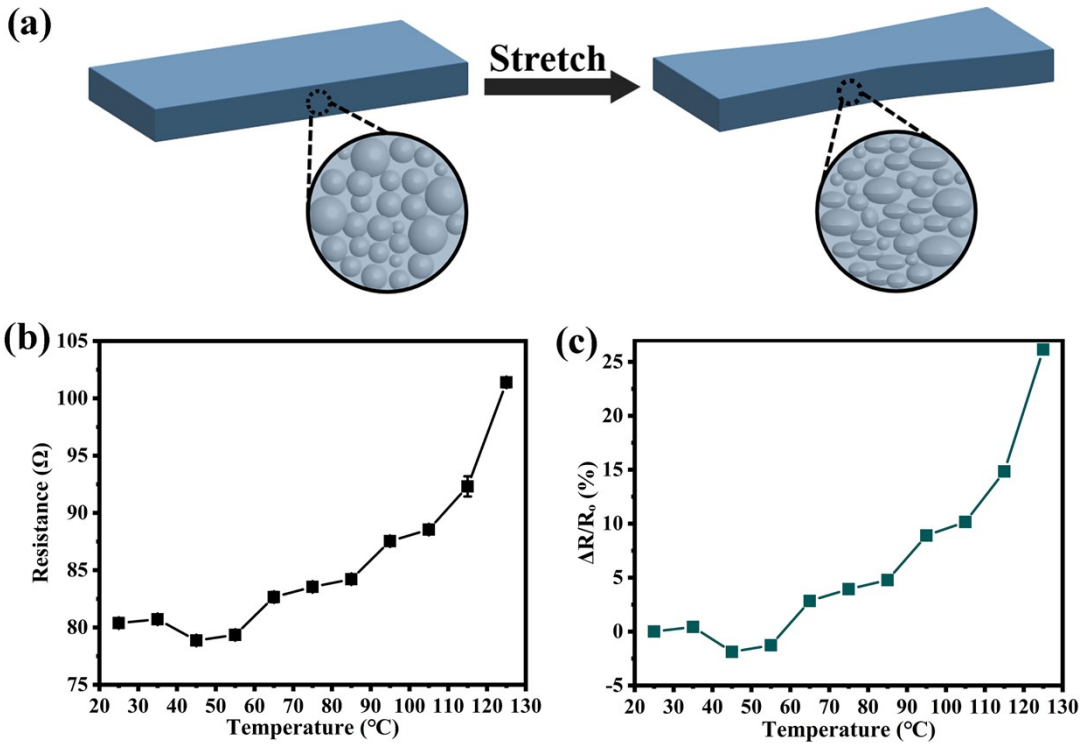

Figure S9. Schematic of the arrangement and shape change of LM micro-droplet particles in WPU-FM/LM composite film during stretching (a). Resistances (b) and relative resistance changes (c) of WPU-FM/LM 0.45 under different temperatures.

Table S1. Elemental composition of the samples.

Sample	Atomic (wt. %)		
	C	N	O
WPU	69.31	2.17	28.52
WPU-F	72.75	2.05	25.20
WPU-M	67.75	2.11	30.14
WPU-FM	72.73	1.93	25.34

Table S2. The healing efficiency of WPU-FM film under different conditions.

WPU-FM		Self-healing efficiency (%)	Tensile strength (MPa)	Elongation at break (%)
80 ℃	12 h	27.94	5.89	22.65
	24 h	73.50	15.50	182.00
85 ℃	24 h	71.41	18.85	451.72
90 ℃	12 h	99.78	21.05	348.87
	24 h	104.32	23.15	360.04
	36 h	109.43	24.28	353.00
100 ℃	6 h	77.51	17.20	326.67
	12 h	79.28	17.59	342.50
110 ℃	6 h	82.03	18.20	360.00
	12 h	83.13	18.45	393.33